Available online at www.sciencedirect.com
SCIENCE DIRECT
Bioorganic & Medicinal Chemistry 14 (2006) 6055–6064
Bioorganic & Medicinal Chemistry

The binding of 3′-*N*-piperidine-4-carboxyl-3′-deoxy-*ara*-uridine to ribonuclease A in the crystal

Demetres D. Leonidas,[a,*] Tushar Kanti Maiti,[c] Anirban Samanta,[c] Swagata Dasgupta,[c] Tanmaya Pathak,[c] Spyros E. Zographos[a] and Nikos G. Oikonomakos[a,b]

[a]*Institute of Organic and Pharmaceutical Chemistry, The National Hellenic Research Foundation, 48 Vas. Constantinou Avenue, 11635 Athens, Greece*
[b]*Institute of Biological Research and Biotechnology, The National Hellenic Research Foundation, 48 Vas. Constantinou Avenue, 11635 Athens, Greece*
[c]*Department of Chemistry, Indian Institute of Technology, Kharagpur 721302, India*

Received 15 March 2006; revised 28 April 2006; accepted 3 May 2006
Available online 30 May 2006

Abstract—The binding of a moderate inhibitor, 3′-*N*-piperidine-4-carboxyl-3′-deoxy-*ara*-uridine, to ribonuclease A has been studied by X-ray crystallography at 1.7 Å resolution. Two inhibitor molecules are bound in the central RNA binding cavity of RNase A exploiting interactions with residues from peripheral binding sites rather than from the active site of the enzyme. The uracyl moiety of the first inhibitor molecule occupies the purine-preferring site of RNase A, while the rest of the molecule projects to the solvent. The second inhibitor molecule binds with the carboxyl group at the pyrimidine recognition site and the uridine moiety exploits interactions with RNase A residues Lys66, His119 and Asp121. Comparative structural analysis of the 3′-*N*-piperidine-4-carboxyl-3′-deoxy-*ara*-uridine complex with other RNase A–ligand complexes provides a structural explanation of its potency. The crystal structure of the RNase A–3′-*N*-piperidine-4-carboxyl-3′-deoxy-*ara*-uridine complex provides evidence of a novel ligand-binding pattern in RNase A for 3′-*N*-aminonucleosides that was not anticipated by modelling studies, while it also suggests ways to improve the efficiency and selectivity of such compounds to develop pharmaceuticals against pathologies associated with RNase A homologues.

1. Introduction

In the human genome 13 distinct vertebrate-specific ribonuclease (RNase) genes have been identified, all localized in chromosome 14.[1] Ribonucleases (RNases) are enzymes that control, post-transcriptionally, the RNA population in cells. The RNase A superfamily is the only enzyme family restricted to vertebrates.[2] Recent studies indicate that there has been a rapid divergence under an unusual evolutionary pressure and suggest that the lineage might have started as host defence proteins.[1] Several homologues of the mammalian pancreatic RNase A (EC 3.1.27.5) superfamily are also involved in various human pathologies and RNase activity in serum and cell extracts is elevated in a variety of cancers and infectious diseases.[3] Angiogenin, a potent inducer of neovascularization, displays pathological side effects during cancer.[4] It has been proposed that the RNase A superfamily started off from a progenitor with structural similarities to Angiogenin.[2] Two other homologues, eosinophil cationic protein (ECP) and eosinophil derived neurotoxin (EDN), are both involved in the immune response system and inflammatory disorders.[5–7] The pathological functions of these RNase A homologues are linked to their enzymatic activity, a fact that renders them as attractive targets for rational ligand design of potent and selective inhibitors, that could be useful as potential pharmaceutics to combat cancer and inflammatory disorders. Several rational inhibitor design efforts[8–10] that target these enzymes are currently in progress.

The RNase A superfamily comprises pyrimidine-specific secreted endonucleases that degrade RNA through a

Keywords: Ribonuclease A; 3′-*N*-Piperidine-4-carboxyl-3′-deoxy-*ara*-uridine; inhibition; X-ray crystallography; Structure-assisted inhibitor design.
* Corresponding author. Tel.: +30 210 7273841; fax : +30 210 7273831; e-mail: ddl@eie.gr

0968-0896/$ - see front matter © 2006 Elsevier Ltd. All rights reserved.
doi:10.1016/j.bmc.2006.05.011

two-step transphosphorolytic–hydrolytic reaction.[11] Several subsites exist within the central catalytic groove of RNase A, where substrate RNA binds, that are defined as $P_o \ldots P_n$ $R_o \ldots R_n$, and $B_o \ldots B_n$ according to the phosphate, ribose and base of RNA that bind, respectively, (*n* indicates the position of the group with respect to the cleaved phosphate phosphodiester bond where $n = 1$).[12] The central region of the active site ($B_1R_1P_1R_2B_2$) is conserved in all RNases and therefore, structure-assisted inhibitor design studies have focused mainly on the parental protein, RNase A, since inhibitors developed against this enzyme could also inhibit other members of the superfamily.[8] Today several inhibitors, mainly substrate analogues, mono and diphosphate (di)nucleotides with adenine at the 5′ position, and cytosine or uridine at the 3′position of the scissile bond, have been studied.[8,13,14] All these compounds are rather marginal inhibitors with dissociation constants in the mid-to-upper micromolar range. The best inhibitor so far is pdUppA-3′p with K_i values of 27 nM, 180 nM and 360 μM for RNase A, EDN and Angiogenin, respectively,[8,15,16] whereas transition state theory predicts picomolar values for genuine transition states.[3]

The majority of small molecule RNase A inhibitors studied thus far have acidic groups such as phosphate, carboxylate, or sulfate.[10,14] Aminonucleosides like 3′-*N*-piperidine-4-carboxyl-3′-deoxy-*ara*-uridine (**3e**) have been selected for inhibition studies with the view that uridine derivatives with amino groups that have basicities comparable to those of the imidazole of His12 and His119 might be able to perturb the protonating/deprotonating environment of the P_1 subsite and hence inhibit the enzymatic activity of RNase A and Angiogenin.[17] Thus, biochemical and biological studies have led to the identification of 3′-*N*-alkylamino-3′-deoxy-*ara*-uridines as a new class of inhibitors of the enzymatic activity of RNase A and the Angiogenin induced angiogenesis.[17] These compounds are the first that do not have a phosphate or a sulfate group which are reported to inhibit the enzymatic activity of RNase A and Angiogenin induced angiogenesis. Here we present the high resolution (1.7 Å) crystal structure of the RNase A-complexed with **3e**, the most potent RNase A inhibitor from the series of the 3′-*N*-alkylamino-3′-deoxy-*ara*-uridines that were tested,[17] which reveals the structural basis for its potency and indicates ways for improving its selectivity and efficiency. In the crystal structure two molecules of compound **3e** bind at the peripheral binding sites of RNase A rather than the central active site in a mode that differs strikingly from the one anticipated by modeling studies based on previous RNase A complex structures.[17]

2. Results and discussion

2.1. Overall structures

The crystallographic asymmetric unit of the monoclinic RNase A crystals used in this study contains two protein molecules (A and B).[18] For comparison reasons and due to the lack of a crystal structure of free RNase A from monoclinic crystals at cryogenic conditions (100 K) [the previous crystal structure of free RNase A from monoclinic crystals (pdb entry 1AFU) was determined at 2.0 Å, at room temperature[18]], we have determined the structure of free RNase A at 1.5 Å resolution, at 100 K. The 100 K free RNase A structure is similar to that reported previously at 2.0 Å at room temperature.[18] The rms distances between the earlier and the present free RNase A structures are 0.60/0.27, 0.55/0.28 and 0.83/0.70 Å (molecule A/molecule B of the RNase A non-crystallographic dimer) for Cα, main chain atoms and all atoms of 124 equivalent residues, respectively. Most of the amino acid residues in the new structure are very well defined in the electron density map with the exception of the loop region between residues 16 and 24, which has higher temperature factors (average *B* factor = 23.0 Å^2) compared to the rest of the protein residues (average B factor excluding 16–24 loop = 12.1 Å^2). This loop appears to be flexible, as in the room temperature structure,[18] even at 100 K. The side chains of Ser59, Gln69 and Asp83 are found in two alternative conformations. The catalytic site in the free RNase structure is occupied by 18 water molecules which participate in a network of hydrogen bonds involving residues Gln11, His12, Lys41, Asn44, Gln69, Asn71, Val118, His119 and Phe120.

Two inhibitor molecules (I and II) were bound at the peripheral binding sites of molecule A (Fig. 1) of the non-crystallographic RNase A dimer but none in molecule B. This partial binding has also been observed in previous binding studies with monoclinic crystals of RNase A[13,18,19] and might be attributed to the lattice contacts that limit access to the RNA binding sites of

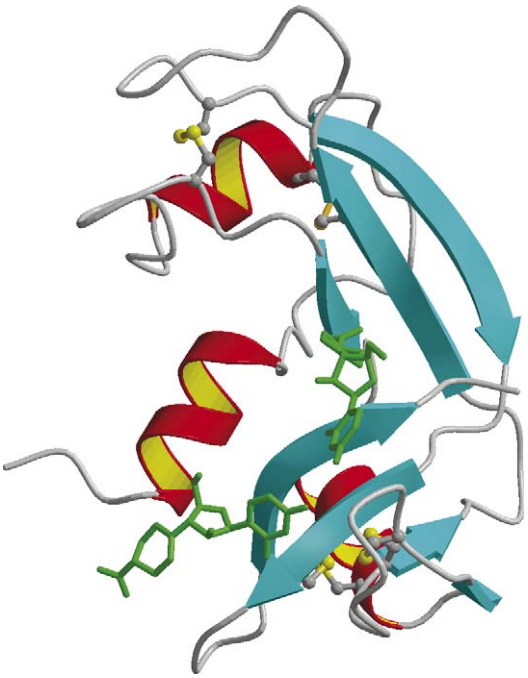

Figure 1. A schematic diagram of the RNase A molecule with the two inhibitor molecules bound.

molecule B in the asymmetric unit. In all free RNase A structures reported so far the side chain of the catalytic residue His119 adopts two conformations denoted as productive ($\chi 1 = \sim 160°$) and non-productive ($\chi 1 = \sim -80°$), which are related by a 100° rotation about the Cα–Cβ bond and a 180° rotation about the Cβ–Cγ bond.[20–23] These conformations are dependent on the pH[24] and the ionic strength of the crystallization solution.[25] In the cryogenic free RNase A structure reported here His119 adopts the non-productive conformation in protein molecule A ($\chi 1 = -51°$) but the productive conformation ($\chi 1 = 173°$) in protein molecule B of the non-crystallographic dimer indicating the diversity of this side chain in the unliganded enzyme structure. Previous studies[26] have shown that binding of ligand groups in P_1 induces the productive conformation of the side chain of His119 and even though in **3e** ligand does not bind at P_1 the side chain of His119 adopts this conformation ($\chi 1 = 159°$).

Upon binding to RNase A, each of the inhibitor molecules I and II displaces six water molecules from the peripheral binding sites of the free enzyme. With the exception of the side chain of His119 that was discussed above, there are no other significant conformational changes in the catalytic site of RNase A upon ligand binding. The rms distances between the structures of free RNase A and the RNase A–**3e** complex are 0.29 Å, 0.31 Å and 0.77 Å for Cα, main chain and all atoms of 124 equivalent residues in RNase A molecule A, respectively.

2.2. The binding of 3e to RNase A

All atoms of the two **3e** molecules (I and II) are well defined within the sigmaA weighted $2F_o - F_c$ electron density map of the RNase A–**3e** complex (Fig. 2).

Upon binding to RNase A, each inhibitor molecule adopts a different conformation. The glycosyl torsion angle χ in both molecules I and II adopts the frequently observed[27] *anti* conformation (Table 1). The ribose adopts the quite rare *O4-endo* puckering in **3e** molecule I, while in molecule II it is found in the preferred, for free and protein bound nucleotides,[27] *C2-endo* conformation. The rest of the backbone torsion angles are in the common range for protein bound pyrimidines[27] with the exception of the torsion angle γ in ligand molecule II which is at the unusual +*ac* range (Table 1). The 4-carboxypiperidine moiety in molecule I adopts the chair conformation, whereas in molecule II it is found in the half-chair conformation (Fig. 2). The numbering scheme used for compound **3e** is shown in Scheme 1.

Inhibitor molecule I binds to RNase A by anchoring its uracyl group to subsite B_2 where it is involved in hydrogen-bond interactions with the side chains of Asn67, Asn71 and Glu111 (Fig. 3A and Table 2). Although the B_2 subsite has been shown to exhibit a strong base preference in the order A > G > C > U,[28] only the interactions of purines in the B_2 site have been examined by crystallography or NMR [complexes with $d(Ap)_4$,[29] d(CpA),[30,31] UpcA,[32,33] 2′,5′, CpA,[31,34] d(ApTpApA),[35] ppA-3′-p, ppA-2′-p[18], 3′,5′ ADP, 2′,5′ ADP, 5′ADP,[13] dUppA-3′-p,[36] pdUppA-3′-p,[15] and IMP[19]], thus far. The RNase A–**3e** complex provides the first structural insights of uracyl binding to B_2. The ribose binds away from subsite R_2 towards the N-terminus of the protein and it is held in place by participating in an extended water-mediated hydrogen-bonding network along with the protein. The 4-carboxypiperidine group is pointing towards the solvent in a location that is probably imposed by the stereochemistry of the ligand (Fig. 3A).

Inhibitor molecule II binds, with the 4-carboxypiperidine moiety, at the subsite B_1 where it is involved in hydrogen-bond interactions through its carboxyl group with Thr45. The uracyl group binds close to subsite P_0 almost parallel to the side chain of Lys66 involved in hydrogen-bond interactions with the side chains of His119 and Asp121 (Fig. 3B and Table 2). RNase A residues and inhibitor atoms are involved in a total of 55 van der Waals contacts (Table 3).

The structural mode of binding of **3e** to RNase A does not resemble any previous binding patterns for other RNase A inhibitors. However, it seems that in **3e** molecule II the carboxyl group imitates the carbonyl groups of uracyl and binds to subsite B_1, whereas the uracyl group binds close to P_1 engaging in hydrogen-bond interactions with His119 and Asp121 and van der Waals interactions with Lys66 (the sole component of subsite P_0). The interaction with Asp121 is also of importance from a mechanistic view since it has been shown that Asp121 serves primarily to orient His119 properly to fulfill its catalytic function,[37] while replacement of Asp121 by Ala in mutation studies[37] diminishes k_{cat}/K_m values for transphosphorylation by about ~100-fold. Thus, it seems that the binding of **3e** to the peripheral binding sites stabilizes the productive conformation of the side chain of His119 through this interaction with Asp121 even though it does not bind directly to subsite P_1. This also provides an explanation to the fact that the side chain of His119 is in this conformation in the ligand complex despite the fact there is no group bound at subsite P_1. The binding of **3e** molecule I seems to be dictated by the docking of uracyl to subsite B_2, while the rest of the molecule projects to the solvent.

Upon binding to RNase A, **3e** molecules I and II become buried (Fig. 4). The solvent accessibilities of the free ligand molecules I and II are 509 $Å^2$ and 506 $Å^2$, respectively. When bound these accessible molecular surfaces shrink to 254 $Å^2$ and 218 $Å^2$, respectively. This indicates that approximately 50% and 57% of the ligand molecule I and II surfaces become buried. The greatest contribution for **3e** molecule I comes from the polar groups that contribute 159 $Å^2$ (62%) of the surface, which becomes inaccessible, whereas for **3e** molecule II, the greatest contribution comes from the non-polar groups that contribute 198 $Å^2$ (69%). On the protein surface, a total of 392 $Å^2$ solvent accessible surface area becomes inaccessible on binding of the two inhibitor molecules. The total buried surface area (protein plus two ligand molecules) for the RNase A–**3e** complex is 909 $Å^2$. The shape correlation statistic

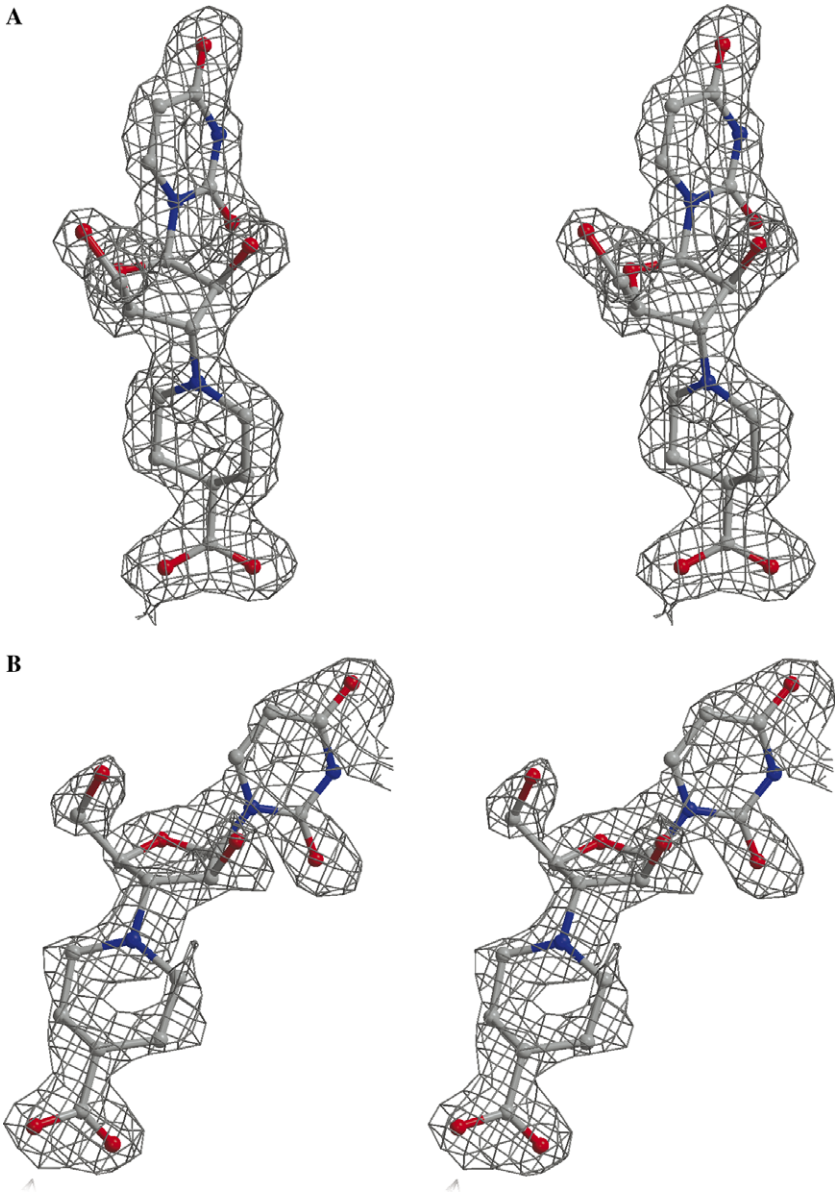

Figure 2. Stereo diagrams of the sigmaA $2|F_o| - |F_c|$ electron density maps calculated from the RNase A model before incorporating the coordinates of the ligand are contoured at 1.0 σ level. The refined structures of the inhibitor are shown for **3e** molecules I (A), and II (B), respectively.

Sc, which is used to quantify the shape complementarity of interfaces and gives an idea of the 'goodness of fit' between two surfaces,[38] is 0.72, and 0.69, for the association to the enzyme of **3e** molecules I and II, respectively, and 0.71 for the combined molecular surface of the two inhibitor molecules.

Although the structure presented here is based on a soaking experiment, data from RNase A co-crystallized with 10 mM **3e** were also available at 2.0 Å resolution. Preliminary analysis of this structure showed that the inhibitor is bound in exactly the same way as in the soaked crystal.

Kinetic studies showed that **3e** is a competitive inhibitor of the enzyme with a K_i = 103 μM at pH 6.0.[17] An electron density map calculated from X-ray data of RNase A crystals, soaked with 0.7 mM of compound **3e** (the highest concentration used for the kinetic experiments[17]) in the crystallization medium for 2 h, showed only **3e** molecule II bound at the peripheral binding site of the enzyme. It seems that this site has a higher affinity for the ligand molecule than the site where ligand molecule I binds, and therefore the inhibition profile observed in the kinetic experiments for compound **3e** corresponds only to the binding of **3e** molecule II to RNase A.

2.3. Comparative structural analysis

Structural superposition of the RNase A–**3e** complex onto the RNase A–pdUppA-3′-p complex reveals that the uridine part of **3e** molecule I superimposes onto the adenosine part, while the 4-carboxypiperidine and the ribose of **3e** molecule II are close to the positions occupied by the uracyl and the 5′phospate group of pdUppA-3′-p (Fig. 5A). The superposition of the RNase

Table 1. Torsion angles for **3e** when bound to RNase A

Inhibitor molecule	I	II
Backbone torsion angles		
O5′–C5′–C4′–C3′ (γ)	68 (+*sc*)	138 (+*ac*)
C5′–C4′–C3′–N7 (δ)	113 (+*ac*)	137 (+*ac*)
C5′–C4′–C3′–C2′	−128	−109
C4′–C3′–C2′–O2′	114	104
Glycosyl torsion angle		
O4′–C1′–N1–C2 (χ)	−133 (*anti*)	−166 (*anti*)
Pseudorotation angles		
C4′–O4′–C1′–C2′ (v_0)	−18	−6
O4′–C1′–C2′–C3′ (v_1)	13	14
C1′–C2′–C3′–C4′ (v_2)	−4	−16
C2′–C3′–C4′–O4′ (v_3)	−6	13
C3′–C4′–O4′–C1′ (v_4)	15	−4
Phase	103 (*O4′-endo*)	162 (*C2′-endo*)

Definitions of the torsion angles are according to the current IUPAC-IUB nomenclature,[51] and the phase angle of the ribose ring is calculated as described previously.[52] For atom definitions, see Scheme 1.

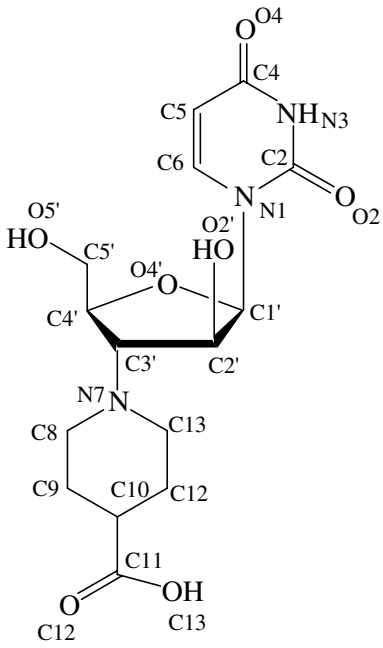

Scheme 1. The chemical structure of **3e** with the numbering scheme used.

A–pdUppA-3′-p complex onto the RNase A–**3e** complex indicates also ways for improving the potency of **3e**. Thus, following the molecular architecture between atom C4′ of the ribose in the adenosine part to the 5′ phosphate group in the uridine part of pdUppA-3′-p (Fig. 5A) we could propose a suitable linker between the 5′ hydroxyl group of **3e** molecule I to the 2′ hydroxyl group of **3e** molecule II. Such a linker might exploit additional interactions with subsite P_1 of the RNase A catalytic site which are not utilised by **3e**.

Superposition of the **3e** complex onto the 3′CMP complex[30] shows that only the carboxyl group of **3e** molecule II superimposes onto the cytidine of 3′CMP (Fig. 5B). Similarly, structural comparison of the binding of **3e** to the binding of araUMP to RNase A, another class of non-natural 3′nucleotide RNase inhibitors identified recently,[14] shows that only the carboxyl moiety of **3e** molecule II binds closely to position of the uracyl ring in the araUMP complex. Both 3′CMP and araUMP exploit interactions with subsite P_1 through their phosphate group which cannot be utilised by compound **3e** since it is lacking such a group. However, the affinity of **3e** for RNase A is comparable to that of 3′CMP (K_i = 103 μM)[39] but much lower than that of araUMP (K_i = 6 μM).[14] The weaker binding of **3e** compared to araUMP could be attributed to the phosphate interactions of araUMP with residues in subsite P_1 which **3e** does not exploit. Based on the similar binding affinities of **3e** and 3′CMP it seems that the binding of the carboxyl group to subsite B_1 imitates well enough the cytidine binding at this subsite, while the hydrogen-bond interactions between the uracyl of **3e** and the side chains of His119 and Asp121 compensate for the lack of interactions with other RNase A residues in subsite P_1 that 3′CMP utilises upon binding to RNase A.

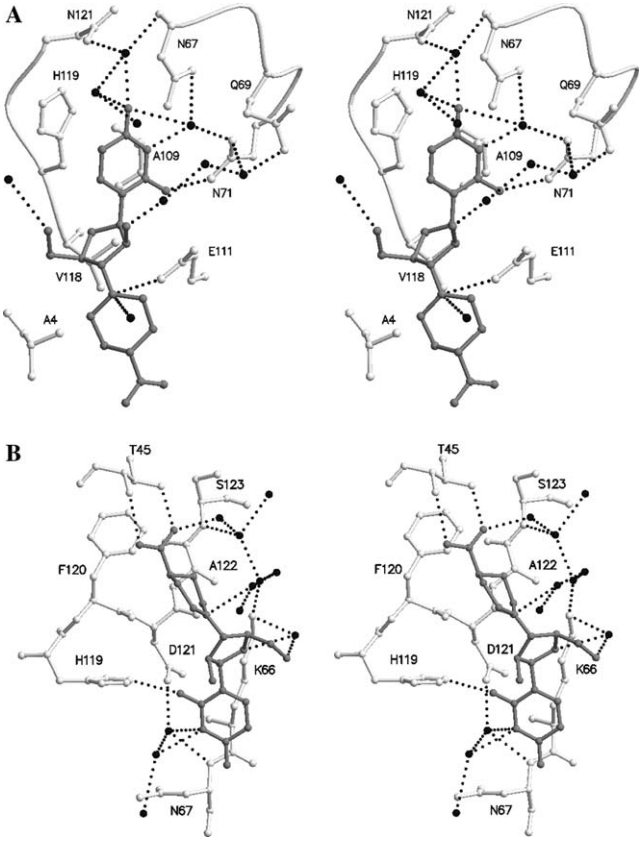

Figure 3. Stereo diagrams of the interactions between RNase A and **3e** molecules I (A), and II (B). The side chains of protein residues involved in ligand binding are shown as ball-and-stick models. Bound waters are shown as black spheres. Hydrogen-bond interactions are represented as dashed lines.

2.4. Modelling

Although the present structure provides a promising starting point for the rational design of tight-binding RNase inhibitors, it also reveals that this process may

Table 2. Potential hydrogen-bond interactions of **3e** when bound to RNase A in the crystal

Inhibitor atom	Ribonuclease A atoms (molecule A)			
	3e molecule I	Distance (Å)	**3e** molecule II	Distance (Å)
O2	Asn71 Nδ2	2.9	His119 Nε2	3.0
N3	Water	2.3	Water	2.8
N3	—	—	Water	3.3
O4	Water	2.6	—	—
O4	Water	2.9	—	—
O4	Water	3.1	—	—
N7	Glu111 Oε1	3.3	Water	3.1
N7	Water	3.4	—	—
O2′	Water	2.6	—	—
O4′	—	—	Water	3.1
O5′	Water	3.2	Water	2.7
O12	—	—	Thr45 Oγ1	2.4
O12	—	—	Water	2.6
O13	—	—	Thr45 N	2.9

Hydrogen-bond interactions were calculated with the program HBPLUS.[53] For ligand atom definitions, see Scheme 1.

Table 3. Potential van der Waals interactions of **3e** upon binding to RNase A

Inhibitor atom	Ribonuclease A atoms (molecule A)	
	3e molecule I	**3e** molecule II
N1	—	Lys66, Cδ
O2	Asn71, Cδ	His119, Cε1
C2	Ala109, Cβ	Lys66, Cβ
N3	Ala109, Cβ	—
C4	Asn67, Nδ2; His119, Cγ, Cδ2	Lys66, Cβ, C
O4	Asn67, Cγ	Asn67, Cα, Cβ
C5	His119, Cβ, Cγ, Nδ1, Cε1, Cδ2	Lys66, Cβ
C6	His119, Cβ, Cγ	Lys66, Cβ, Cδ
C1′	Glu111, Cδ, Oε1, Cγ2	Lys66, Cδ
O4′	Val118, Cγ2	Lys66, Cδ
C4′	Val118, Cβ, Cγ2	—
C2′	Glu111, Cδ, Oε1, Oε2	—
C8	Glu111, Cδ, Oε1	Asp12, C, O
C9	Glu111, Oε1	Phe120, Cδ1
C10	—	Phe120, Cδ1
C11	—	Asn44, Cα, N; Thr45, Cβ, Oγ1; Phe120, Cδ1, Cε1
C12	Ala4, Cβ	—
C13	Ala4, Cβ	—
O12	—	Thr45, Cβ, Oγ1
O13	—	His12, Cε1; Asn44, Cα, C
Total	28 contacts (7 residues)	27 contacts (7 residues)

not follow a predictable course. Initial modelling of the **3e** complex[17] based on the RNase A–3′CMP complex[30] had suggested that only one **3e** molecule would bind to the central active site with the carboxylic group in subsite P_1 and the uridine moiety in subsite B_1. From the present complex structure it is not clear why the uridine part of the **3e** molecule does not bind to the pyrimidine recognition site B_1. Nonetheless, as we have shown, the actual complex structure is quite different indicating that the phosphate recognition subsite P_1 has a low, if any, specificity for carboxyl groups. Furthermore, the previous docking studies[17] estimated a theoretical K_i of 0.09 μM, a value considerably lower than the experimental one (103 μM). Docking studies based on the crystal structure of the **3e** complex are in close agreement with the binding mode observed in the crystal (Fig. 6) and estimate a theoretical K_i of 47 μM, a value that is in a much better agreement with the experimental K_i. These findings may have important implications for RNase inhibitor development as well as for rational design efforts in general and emphasize the importance of obtaining direct structural information on each new inhibitor complex on the optimization pathway.

2.5. Conclusions

The structural basis of the inhibition of RNase A by 3′-*N*-piperidine-4-carboxyl-3′-deoxy-*ara*-uridine (**3e**) has been revealed by X-ray crystallography at 1.7 Å resolution. Two ligand molecules bind to RNase A peripheral binding sites in a novel binding mode. Ligand molecule I binds with its uridine moiety in subsite B_2, while the rest

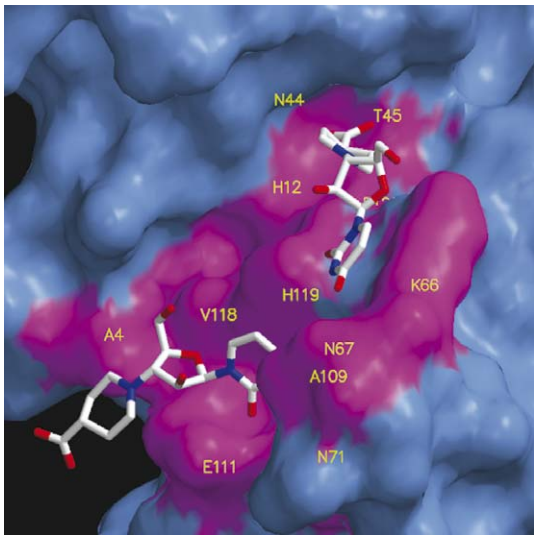

Figure 4. The molecular surface of RNase A calculated using the program GRASP[55] in the vicinity of the RNA binding sites. The inhibitor molecule is shown as a ball-and-stick model. RNase A residues interacting with **3e** are labelled and shown in purple.

of the molecule projects to the solvent. Ligand molecule II binds by anchoring its carboxyl group to subsite B_1, whereas its uracyl group binds close to P_0. Comparative structural analysis of the RNase A–**3e** complex with other RNase A–ligand complexes suggests ways to improve the potency of **3e** and this study could be a starting point for the design of a novel family of inhibitors. Thus, we propose that by connecting the two ligand molecules with a suitable linker that can form additional interactions with the P_1 subsite a much more potent inhibitor can be produced.

3. Materials and methods

3.1. Materials

Bovine pancreatic RNase A (type XII-A) and other chemicals were obtained from Sigma–Aldrich (Athens, Greece). The synthesis of compound **3e** (Scheme 1) was described previously.[17]

3.2. Crystallization, data collection and structure refinement

Crystals of RNase A were grown at 16 °C using the hanging drop vapour diffusion technique as described previously.[18] Crystals of the inhibitor complexes were obtained by soaking the RNase A crystals in 20 mM sodium citrate, pH 5.5, 25% PEG 4000 containing 46 mM **3e** for 5.5 h, prior to data collection.

Diffraction data for the free RNase A and the inhibitor complex to 1.5 Å and 1.7 Å resolution, respectively, were collected on station X13 ($\lambda = 0.8068$ Å) EMBL/DESY, Hamburg, at 100 K, using a MAR CCD detector. Data were processed using the HKL package[40] and intensities were transformed to amplitudes by the program TRUNCATE.[41] Phases were obtained using the structure of free RNase A from monoclinic crystals at 100 K as starting model. Alternate cycles of manual building with the program O,[42] and refinement using the maximum likelihood target function as implemented in the program REFMAC,[43] improved the model. Inhibitor molecules were modelled using the Dundee PRODRG server (http://davapc1.bioch.dundee.ac.uk/programs/prodrg/) and they were included in the refine-

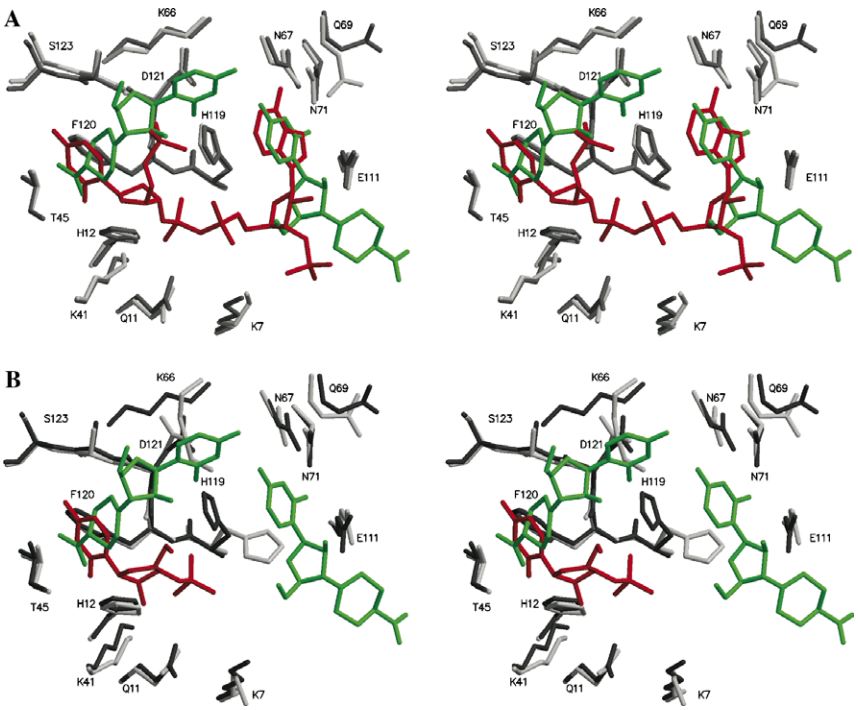

Figure 5. Structural comparisons of the RNase A–**3e** (grey) complex and RNase A–pdUppA-3′p (A), RNase A –3′CMP (B), complexes (white). Ligand molecules are shown in colour; **3e** green, pdUppA-3′p and 3′CMP red.

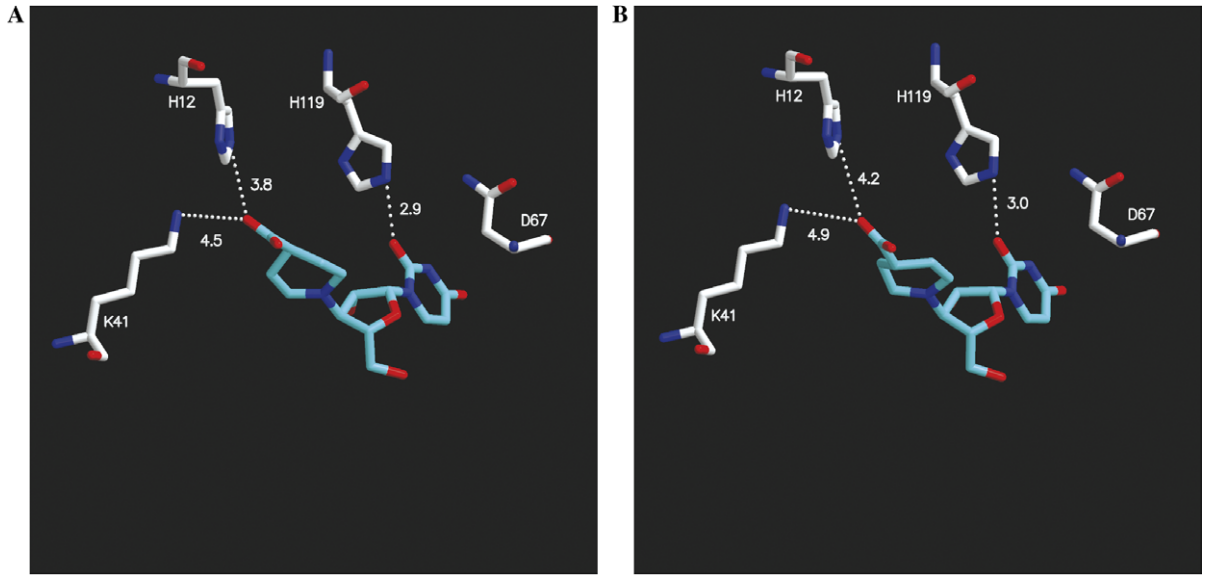

Figure 6. The interactions of the docked (A) and bound (B) inhibitor molecule II of **3e** with protein residues. Selected distances are represented as dashed lines and numbers shown are in angstrom.

ment procedure during its final stages. A final round of TLS (Translation/Libration/Screw) refinement within the program REFMAC[43] using TLS groups for the protein generated by the TLSMD web server[44] improved considerably the final model. Details of data processing and refinement statistics are provided in Table 4.

The program PROCHECK[45] was used to assess the quality of the final structure. Analysis of the Ramachandran (φ–ψ) plot showed that all residues lie in the allowed regions. Solvent accessible areas were calculated with the program NACCESS.[46] Atomic coordinates of the free RNase A and the inhibitor complex have been deposited in Research Collaboratory for Structural Bioinformatics Protein Data Bank, (http://www.rcsb.org) with accession numbers 2G8Q and 2G8R, respectively. Figures were prepared with the programs MOLSCRIPT[47] or BOBSCRIPT[48] and rendered with Raster3D.[49]

3.3. Docking

The Cartesian coordinates (protein and molecule II of ligand **3e**) obtained from the crystal complex were used for the docking analysis using the program AutoDock 3.0.[50] Water molecules were removed from the protein PDB file, polar hydrogen atoms were added and Kollman United Atomic (KOLLUA) charges were assigned. A grid size of $90 \times 90 \times 90$ Å^3 with a grid spacing of 0.25 Å and centered at atom C3′ of ligand, that was automatically chosen as the rigid root by the program, was used. Ligand docking was carried out with the

Table 4. Crystallographic statistics

Structure	RNase A	RNase A–**3e** complex
Resolution (Å)	30.0–1.5	30.0–1.7
Outermost shell (Å)	1.54–1.50	1.75–1.70
Reflections measured	268,419	471,750
Unique reflections	37,534	24,227
R_{symm}[a]	0.029 (0.130)	0.071 (0.450)
Completeness (%)	99.3 (99.7)	99.3 (98.7)
$\langle I/\sigma I \rangle$	3.7 (3.7)	4.5 (3.2)
R_{cryst}[b]	0.185 (0.200)	0.191 (0.286)
R_{free}[c]	0.218 (0.223)	0.230 (0.337)
No of solvent molecules	373	262
rms deviation from ideality		
in bond lengths (Å)	0.008	0.009
in angles (°)	1.2	1.3
Average *B* factor		
Protein atoms (Å^2) (molecule A/molecule B)	12.7/13.7	20.3/17.9
Solvent molecules (Å^2)	29.1	33.1
Ligand atoms (Å^2) (molecule I/molecule II)	—	34.3/24.9

[a] $R_{\text{symm}} = \Sigma_h \Sigma_i |I(h) - I_i(h)| / \Sigma_h \Sigma_i I_i(h)$, where $I_i(h)$ and $I(h)$ are the ith and the mean measurements of the intensity of reflection h.
[b] $R_{\text{cryst}} = \Sigma_h ||F_o| - |F_c|| / \Sigma_h |F_o|$, where F_o and F_c are the observed and calculated structure factors' amplitudes of reflection h, respectively.
[c] R_{free} is equal to R_{cryst} for a randomly selected 5% subset of reflections not used in the refinement.[54] Values in parentheses are for the outermost shell.

AutoDock 3.0.5 Lamarckian Genetic Algorithm (GA).[50] The ligand conformation was kept rigid, that is, the ligand had only translation and orientation movement but no torsional movement. The approximate binding free energies calculated by this program are based on an empirical function derived by linear regression analysis of protein–ligand complexes with known binding constants. This function includes terms for changes in energy due to van der Waals, hydrogen bonding and electrostatic forces, as well as ligand torsion and desolvation. The docked energy also includes the ligand internal energy or the intramolecular interaction energy of the ligand. Since the ligand was considered as a rigid one, the two energy terms 'final internal energy of ligand' and 'torsional free energy' become zero. For this reason 'estimated free energy of binding' and 'final docked energy' are same. This value is −5.90 kcal/mol and 'estimated inhibition constant' K_i is 4.7×10^{-5} M at 298.15 K. The root mean square deviation (rmsd) value for the ligand molecule between the model and the crystal structure is 0.47 Å.

Acknowledgments

We thank Mr. G.N. Hatzopoulos for help in the crystallization experiments. The assistance of the staff at EMBL, Hamburg, and S.R.S., Daresbury, is also acknowledged for providing excellent facilities for X-ray data collection. This work was supported by the Hellenic General Secretariat for Research and Technology (GSRT), through a Joint Research and Technology project between Greece and Slovenia (2002–2005) (to D.D.L.). S.D.G. and T.P. are grateful to Department of Science and Technology (DST), Government of India, for financial support (SR/S5/OC-13/2002). T.K.M. thanks CSIR, India, for a fellowship. This work was also supported by grants from European Community—Research Infrastructure Action under the FP6 'Structuring the European Research Area Programme' for work at the Synchrotron Radiation Source, CCLRC, Daresbury, U.K. (Contract Number HPRI-CT-1999-00012), and EMBL Hamburg Outstation, Germany (contract number RII3/CT/2004/5060008), to D.D.L and N.G.O.

References and notes

1. Cho, S.; Beintema, J. J.; Zhang, J. *Genomics* **2005**, *85*, 208.
2. Cho, S.; Zhang, J. *Gene* **2006**.
3. Loverix, S.; Steyaert, J. *Curr. Med. Chem.* **2003**, *10*, 779.
4. Riordan, J. F. *Methods Enzymol.* **2001**, *341*, 263.
5. Rosenberg, H. F.; Domachowske, J. B. *J. Leukocyte Biol.* **2001**, *70*, 691.
6. Rosenberg, H. F.; Domachowske, J. B. *Methods Enzymol.* **2001**, *341*, 273.
7. Venge, P.; Bystrom, J.; Carlson, M.; Hakansson, L.; Karawacjzyk, M.; Peterson, C.; Seveus, L.; Trulson, A. *Clin. Exp. Allergy* **1999**, *29*, 1172.
8. Russo, A.; Acharya, K. R.; Shapiro, R. *Methods Enymol.* **2001**, *341*, 629.
9. Jenkins, J. L.; Kao, R. Y.; Shapiro, R. *Proteins* **2003**, *50*, 81.
10. Jenkins, J. L.; Shapiro, R. *Biochemistry* **2003**, *43*, 6674.
11. Beintema, J. J.; Kleineidam, R. G. *Cell. Mol. Life Sci.* **1998**, *54*, 825.
12. Raines, R. T. *Chem. Rev.* **1998**, *98*, 1045.
13. Leonidas, D. D.; Chavali, G. B.; Oikonomakos, N. G.; Chrysina, E. D.; Kosmopoulou, M. N.; Vlassi, M.; Frankling, C.; Acharya, K. R. *Protein Sci.* **2003**, *12*, 2559.
14. Jenkins, C. L.; Thiyagarajan, N.; Sweeney, R. Y.; Guy, M. P.; Kelemen, B. R.; Acharya, K. R.; Raines, R. T. *FEBS J.* **2005**, *272*, 744.
15. Leonidas, D. D.; Shapiro, R.; Irons, L. I.; Russo, N.; Acharya, K. R. *Biochemistry* **1999**, *38*, 10287.
16. Russo, N.; Shapiro, R. *J. Biol. Chem.* **1999**, *274*, 14902.
17. Maiti, T. K.; Soumya, D.; Dasgupta, S.; Pathak, T. *Bioorg. Med. Chem.* **2006**, *14*, 1221.
18. Leonidas, D. D.; Shapiro, R.; Irons, L. I.; Russo, N.; Acharya, K. R. *Biochemistry* **1997**, *36*, 5578.
19. Hatzopoulos, G. N.; Leonidas, D. D.; Kardakaris, R.; Kobe, J.; Oikonomakos, N. G. *FEBS J.* **2005**, *272*, 3988.
20. Borkakoti, N.; Moss, D. A.; Palmer, R. A. *Acta Crystallogr.* **1982**, *B38*, 2210.
21. Howlin, B.; Moss, D. S.; Harris, G. W. *Acta Crystallogr.* **1989**, *A45*, 851.
22. deMel, V. S. J.; Doscher, M. S.; Martin, P. D.; Edwards, B. F. P. *FEBS Lett.* **1994**, *349*, 155.
23. Mazzarella, L.; Capasso, S.; Demasi, D.; Di'Lorenzo, G.; Mattia, C. A.; Zagari, A. *Acta Crystallogr.* **1993**, *D49*, 389.
24. Berisio, R.; Lamzin, V. S.; Sica, F.; Wilson, K. S.; Zagari, A.; Mazzarella, L. *J. Mol. Biol.* **1999**, *292*, 845.
25. Fedorov, A. A.; Joseph-McCarthy, D.; Fedorov, E.; Sirakova, D.; Graf, I.; Almo, S. C. *Biochemistry* **1996**, *35*, 15962.
26. Borkakoti, N. *Eur. J. Biochem.* **1983**, *132*, 89.
27. Moodie, S. L.; Thornton, J. M. *Nucleic Acids Res.* **1993**, *21*, 1369.
28. Witzel, H.; Barnard, E. A. *Biochem. Biophys. Res. Commun.* **1962**, *7*, 295.
29. McPherson, A.; Brayer, G. D.; Morrison, R. D. *J. Mol. Biol.* **1986**, *189*, 305.
30. Zegers, I.; Maes, D.; Dao-Thi, M.-H.; Poortmans, F.; Palmer, R.; Wyns, L. *Protein Sci.* **1994**, *31*, 2322.
31. Toiron, C.; Gonzalez, C.; Bruix, M.; Rico, M. *Protein Sci.* **1996**, *5*, 1633.
32. Richards, F. M.; Wyckoff, H. W.; Ribonuclease, S. In *Atlas of Molecular Structures in Biology*; Philips, D. C., Richards, F. M., Eds.; Clarendon: Oxford, UK, 1973; Vol. 1.
33. Gilliland, G. L.; Dill, J.; Pechik, I.; Svensson, L. A.; Sjolin, L. *Protein Pept. Lett.* **1994**, *1*, 60.
34. Wodak, S. Y.; Liu, M. Y.; Wyckoff, H. W. *J. Mol. Biol.* **1977**, *116*, 855.
35. Fontecilla-Camps, J. C.; de Llorens, R.; le Du, M. H.; Cuchillo, C. M. *J. Biol. Chem.* **1994**, *269*, 21526.
36. Jardine, A. M.; Leonidas, D. D.; Jenkins, J. L.; Park, C.; Raines, R. T.; Acharya, K. R.; Shapiro, R. *Biochemistry* **2001**, *40*, 10262.
37. Schultz, L. W.; Quirk, D. J.; Raines, R. T. *Biochemistry* **1998**, *37*, 8886.
38. Lawrence, M. C.; Colman, P. M. *J. Mol. Biol.* **1993**, *234*, 946.
39. Anderson, D. G.; Hammes, G. G.; Walz, F. G. *Biochemistry* **1968**, *7*, 1637.
40. Otwinowski, Z.; Minor, W. Processing of X-ray diffraction data collected in oscillation mode. In *Methods in Enzymology*; Carter, C. W. J., Sweet, R. M., Eds.; Academic Press: New York, 1997; Vol. 276, p 307.
41. French, S.; Wilson, K. S. *Acta Crystallogr.* **1978**, *A34*, 517.

42. Jones, T. A.; Zou, J. Y.; Cowan, S. W.; Kjeldgaard, M. *Acta Crystallogr.* **1991**, *A47*, 110.
43. Murshudov, G. N.; Vagin, A. A.; Dodson, E. J. *Acta Crystallogr.* **1997**, *D53*, 240.
44. Painter, J.; Merritt, E. A. *J. Appl. Crystallogr.* **2005**, *39*, 109.
45. Laskowski, R. A.; MacArthur, M. W.; Moss, D. S.; Thornton, J. M. *J. Appl. Crystallogr.* **1993**, *26*, 283.
46. Hubbard, S. J.; Thornton, J. M. NACCESS, Computer Program, Department of Biochemistry and Molecular Biology, University College London, **1993**.
47. Kraulis, P. J. *J. Appl. Crystallogr.* **1991**, *24*, 946.
48. Esnouf, R. M. *J. Mol. Graphics Model.* **1997**, *15*, 132.
49. Merritt, E. A.; Bacon, D. J. *Macromol. Crystallogr.* **1997**, *B277*, 505.
50. Morris, G. M.; Goodsell, D. S.; Halliday, R. S.; Huey, R.; Hart, W. E.; Belew, R. K.; Olson, A. J. *J. Comput. Chem.* **1998**, *19*, 1639.
51. IUPAC-IUB, *Eur. J. Biochem.* **1983**, *131*, 9.
52. Altona, C.; Sundaralingam, M. *J. Am. Chem. Soc.* **1972**, *94*, 8205.
53. McDonald, I. K.; Thornton, J. M. *J. Mol. Biol.* **1994**, *238*, 777.
54. Brünger, A. T. *Nature* **1992**, *355*, 472.
55. Nicholls, A.; Honig, B. *J. Comput. Chem.* **1991**, *12*, 435.